The Journal of Chemical Physics

RESEARCH ARTICLE | MARCH 05 2024

Hyperfine and Zeeman interactions in ultracold collisions of molecular hydrogen with atomic lithium

Hubert Jóźwiak ; Timur V. Tscherbul ; Piotr Wcisło

J. Chem. Phys. 160, 094304 (2024)
https://doi.org/10.1063/5.0193148

AIP Publishing

The Journal of Chemical Physics ARTICLE pubs.aip.org/aip/jcp

Hyperfine and Zeeman interactions in ultracold collisions of molecular hydrogen with atomic lithium

Cite as: J. Chem. Phys. 160, 094304 (2024); doi: 10.1063/5.0193148
Submitted: 21 December 2023 • Accepted: 8 February 2024 •
Published Online: 5 March 2024

Hubert Jóźwiak,[1,a)] Timur V. Tscherbul,[2] and Piotr Wcisło[1]

AFFILIATIONS

[1] Institute of Physics, Faculty of Physics, Astronomy and Informatics, Nicolaus Copernicus University in Toruń, Grudziądzka 5, 87-100 Toruń, Poland

[2] Department of Physics, University of Nevada, Reno, Nevada 89557, USA

[a)] **Author to whom correspondence should be addressed:** hubert.jozwiak@doktorant.umk.pl

ABSTRACT

We present a rigorous quantum scattering study of the effects of hyperfine and Zeeman interactions on cold Li–H_2 collisions in the presence of an external magnetic field using a recent *ab initio* potential energy surface. We find that the low-field-seeking states of H_2 predominantly undergo elastic collisions: the ratio of elastic-to-inelastic cross sections exceeds 100 for collision energies below 100 mK. Furthermore, we demonstrate that most inelastic collisions conserve the space-fixed projection of the nuclear spin. We show that the anisotropic hyperfine interaction between the nuclear spin of H_2 and the electron spin of Li can have a significant effect on inelastic scattering in the ultracold regime, as it mediates two processes: the electron spin relaxation in lithium and the nuclear spin–electron spin exchange. Given the predominance of elastic collisions and the propensity of inelastic collisions to retain H_2 in its low-field-seeking states, our results open up the possibility of sympathetic cooling of molecular hydrogen by atomic lithium, paving the way for future exploration of ultracold collisions and high-precision spectroscopy of H_2 molecules.

I. INTRODUCTION

Cold collisions and chemical reactions involving molecular hydrogen have been the subject of much theoretical and experimental interest due to their significance in astrochemistry and cold controlled chemistry.[1,2] In particular, the $F + H_2 \rightarrow HF + H$ reaction, despite having a high energetic barrier of ~800 K, occurs quite efficiently in cold environments (10–100 K) and is the only known source of HF in the interstellar medium.[3] Experiments on the Penning ionization of H_2 upon collisions with metastable (^{3}S) helium revealed sub-K shape resonances,[4] isotopic effects,[5] and a significant role of molecular rotation[6] and anisotropy of the molecule–atom interaction[7] in cold reaction dynamics. Cold collisions of vibrationally excited isotopologues of molecular hydrogen (HD and D_2) with D_2,[8,9] H_2,[9] and He[10,11] revealed interesting stereodynamic effects,[12] interference patterns, and shape resonances, which enable the quantum interference-based coherent control of the collision outcome.[13,14]

Previous theoretical studies of cold collisions involving molecular hydrogen and its isotopologues[12,15–25] neglected the effects of hyperfine interactions and Zeeman shifts on collisions with H_2, which could be substantial at ultralow temperatures. For instance, the hyperfine splitting of the $v = 0, N = 1$ state in *ortho*-H_2 is ~600 kHz[26–28] (or k_B 20 μK). The hyperfine structure of this state in an external magnetic field is quite complex, comprising nine Zeeman states.[26] However, ultracold collision dynamics involving these states and the mechanisms driving particular transitions (e.g., nuclear spin relaxation) remain unexplored.

An additional motivation to study the role of hyperfine and Zeeman interactions in cold collisions of H_2 molecules is related to high-precision spectroscopy of molecular hydrogen. Accurate determination of energy intervals between rovibrational states in hydrogen (with a relative accuracy reaching the sub-ppb level[29,30]) allows for performing stringent tests of quantum electrodynamics[31–33] and for putting constraints on the strength of hypothetical interactions beyond the standard model.[34] To overcome Doppler broadening

and enhance the precision of the determined transition frequencies, experimental groups employ saturation techniques,[35,36] molecular beams[29,30] or cooling of the gas sample[37–39] (down to 57 K). Further improvement in high-precision spectroscopy would be possible if molecular hydrogen could be cooled and trapped. Recently, we proposed a scheme for implementing a magic wavelength for the fundamental transition $v = 0, N = 0 \rightarrow v = 1, N = 2$ in *para*-H_2[40] (which is not magnetically trappable) that has a potential to enable much higher accuracy. In contrast, magnetic trapping could be used to increase the precision spectroscopy of the fundamental transition $(v = 0, N = 1 \rightarrow v = 1, N = 1)$ in *ortho*-H_2. Both the optical dipole and magnetic traps could reach depths of the order of 1 mK, for the laser power density of 1 MW/mm^2 and magnetic field strength of 0.4 T, respectively (as recently demonstrated in Ref. 41, it is possible to use strong and focused laser beams to achieve trap depths of ~3.6 K for H_2). Further progress in high-precision spectroscopy is contingent upon the ability to cool H_2 far below 1 mK.

One such possibility is sympathetic cooling, which relies on immersing a molecular system in a gas of coolant atoms, preferably of a similar mass.[42–45] Under such conditions, elastic collisions result in cooling by transferring momentum between molecules and the coolant atoms. In contrast, inelastic collisions can cause transitions to high-field-seeking (untrappable) states, which release the internal energy stored in these states, and lead to heating and trap loss.[44,45] For efficient sympathetic cooling, the ratio of the cross section for elastic to inelastic collisions $(\gamma = \sigma_{\rm el}/\sigma_{\rm inel})$ should be larger than 100.[46]

A relatively small mass and the fact that it can be cooled down to the μK regime using laser cooling techniques make atomic lithium an attractive candidate for sympathetic cooling of H_2. Duarte *et al.*[47] have demonstrated a magneto-optical trap (MOT) for ^{6}Li atoms operating on a narrow $2S_{1/2} \rightarrow 3P_{3/2}$ transition at 323 nm, achieving temperatures as low as 59 μK. However, the feasibility of sympathetic cooling of H_2 by collisions with Li remains to be determined. For instance, there is a significant mismatch in the Zeeman splittings of the two species, which could lead to losses once the lithium MOT and a hypothetical magnetic trap of H_2 are overlapped. Furthermore, it is unclear whether the ratio, γ, of the cross section for elastic to inelastic collisions of H_2 with Li is high enough to support the cooling process. In order to accurately calculate γ, it is necessary to take into account the effects of hyperfine interactions and the presence of an external magnetic field.

In this paper, we present the first rigorous theoretical study of the role of hyperfine and Zeeman interaction effects in cold atom–H_2 collisions. We investigate the cold collisions of *ortho*-H_2 $(v = 0, N = 1)$ molecules with ^{6}Li atoms using coupled-channel quantum scattering calculations based on a highly accurate *ab initio* potential energy surface (PES).[48] In the field-free case, we find that the three hyperfine states of H_2 are collisionally stable, i.e., the ratio of cross sections for elastic (F-conserving) to inelastic (F-changing) collisions exceeds 100, with the exception of a narrow range in the vicinity of a g-wave shape resonance located at $E \approx k_B \times 1.2$ K. We find that the presence of the magnetic dipolar interaction between the nuclear magnetic moment of H_2 and the electron spin magnetic moment of Li manifests itself in the ultracold regime, where it drastically increases the inelastic $F = 0 \rightarrow F' = 1$ scattering (otherwise suppressed by the selection rules for transitions driven by the H_2–Li interaction potential). We also perform quantum scattering calculations in an external magnetic field, and we analyze relaxation from the three low-field-seeking Zeeman states in H_2 upon collisions with ^{6}Li atoms in the trappable $(S = 1/2, M_S = 1/2)$ state. We find that the inelastic relaxation is dominated by collisions that conserve the space-fixed projection of the nuclear spin of H_2. The magnetic dipolar interaction drives the relaxation of the electronic spin of Li, which has profound consequences on the possibility of sympathetic cooling of H_2 by lithium.

This article is organized as follows: In Sec. II, we outline the quantum theory of collisions between $^1\Sigma$ molecules with two magnetic nuclei (such as *ortho*-H_2) and ^2S atoms in an external magnetic field, which includes the intramolecular hyperfine interactions in the $^1\Sigma$ molecules, as well as the spin-dependent (SD) interaction between the molecule and the ^2S atom. Next, we apply this theory to cold Li–H_2 collisions in Sec. III, where we present and discuss the results for the field-free case. Then, in Sec. IV, we provide the state-to-state cross sections for transitions between the Zeeman sublevels of *ortho*-H_2 in an external magnetic field. We discuss the kinetic energy and magnetic field dependence of the cross sections, as well as the implications of the calculated elastic-to-inelastic scattering ratio on the possibility of sympathetic cooling of H_2 by ^{6}Li. Section V concludes by summarizing the main results of this work. Atomic units are used throughout this article unless stated otherwise.

II. THEORY

Here, we present the quantum theory of collisions between a $^1\Sigma$ molecule and a ^2S atom in the presence of an external magnetic field. The theory is based on the seminal work of Krems and Dalgarno[49] and Volpi and Bohn,[50] who first considered diatom–atom collisions in a magnetic field. It is also an extension of the recent work of Hermsmeier *et al.*[51] (who studied nuclear spin relaxation in cold He–^{13}C^{16}O collisions) to the case of collisions of open-shell atoms, such as ^{6}Li, and molecules with two magnetic nuclei, such as *ortho*-H_2.

We use space-fixed Jacobi coordinates to describe the scattering system: the separation vector $\mathbf{R}$ from the atom to the center of mass of the H_2 molecule, the internuclear vector $\mathbf{r}$, and the angle θ between $\mathbf{R}$ and $\mathbf{r}$. There are six angular momenta in the $H_2(^1\Sigma_g^+)$–Li(^2S) system: the rotational angular momentum of the nuclei in H_2 ($\hat{\mathbf{N}}$); the nuclear spin angular momenta of the protons, $\hat{\mathbf{I}}_1$ and $\hat{\mathbf{I}}_2$ ($I_i = |\hat{\mathbf{I}}_i| = 1/2$, $i = 1, 2$); the total electron spin of the lithium atom, $\hat{\mathbf{S}}$ ($S = |\hat{\mathbf{S}}| = 1/2$); the nuclear spin angular momentum of lithium, $\hat{\mathbf{I}}_{\rm Li}$ ($I_{\rm Li} = |\hat{\mathbf{I}}_{\rm Li}| = 1$ for ^{6}Li and 3/2 for ^{7}Li); and the angular momentum operator describing the orbital motion of the collision partners, $\hat{\boldsymbol{l}}$. For reasons clarified below, we neglect the hyperfine structure of lithium and we exclude $\hat{\mathbf{I}}_{\rm Li}$ from the analysis. We couple the two nuclear spins of the protons to form the total nuclear spin of H_2, $\hat{\mathbf{I}}_{H_2} = \hat{\mathbf{I}}_1 + \hat{\mathbf{I}}_2$. We recall that molecular hydrogen exists in two spin isomeric forms: *para*-H_2 with $I_{H_2} = |\hat{\mathbf{I}}_{H_2}| = 0$ and *ortho*-H_2 with $I_{H_2} = |\hat{\mathbf{I}}_{H_2}| = 1$. Because the total wave function of H_2 must be antisymmetric with respect to the permutation of the protons, *para*-H_2 exhibits a rotational structure with only even values of $N = |\hat{\mathbf{N}}|$, while the rotational structure of *ortho*-H_2 involves only odd N values. Since $I_{H_2} = 0$ for *para*-H_2, this spin isomer does not have the hyperfine structure and nuclear Zeeman shifts and interacts with the magnetic field only through its weak rotational magnetic moment (for $N = 0$ *para*-H_2, the rotational magnetic moment is strictly zero).

In contrast, *ortho*-H_2 does have a non-zero nuclear spin, yielding stronger Zeeman shifts that make it amenable to magnetic trapping. Thus, we focus on *ortho*-H_2 in what follows.

The Hamiltonian for the atom–molecule collision system is

$$\hat{H} = -\frac{1}{2\mu R}\frac{\partial^2}{\partial R^2}R + \frac{\hat{\mathbf{l}}^2}{2\mu R^2} + \hat{V}(\mathbf{R},\mathbf{r}) + \hat{V}_{\mathrm{SD}}(\mathbf{R},\mathbf{r},\hat{\mathbf{I}},\hat{\mathbf{S}}) + \hat{H}_{\mathrm{as}}, \quad (1)$$

where $\mu = m_{\mathrm{at}}m_{\mathrm{mol}}/(m_{\mathrm{at}} + m_{\mathrm{mol}})$ is the reduced mass of the collision partners (we use $m_{\mathrm{at}} = 6.015\,121$ and $m_{\mathrm{mol}} = 2.015\,65$ atomic mass units),[52] $\hat{V}(\mathbf{R},\mathbf{r})$ is the atom–molecule potential energy surface, and $\hat{V}_{\mathrm{SD}}(\mathbf{R},\mathbf{r},\hat{\mathbf{I}},\hat{\mathbf{S}})$ denotes the spin-dependent (SD) Hamiltonian (note that the subscript in $\hat{\mathbf{I}}_{\mathrm{H_2}}$ is dropped for simplicity, and the nuclear spin of H_2 is denoted simply as $\hat{\mathbf{I}}$),

$$\hat{V}_{\mathrm{SD}}(\mathbf{R},\mathbf{r},\hat{\mathbf{I}},\hat{\mathbf{S}}) = \sum_{i=1,2} A_F^i(\mathbf{R},\mathbf{r})\hat{\mathbf{I}}_i\cdot\hat{\mathbf{S}} + \sum_{i=1,2}\sum_{\alpha,\beta} c^i_{\alpha\beta}(\mathbf{R},\mathbf{r})\hat{\mathbf{I}}_{i_\alpha}\hat{\mathbf{S}}_\beta, \quad (2)$$

in which the sum over i involves the two protons in H_2 and α and β run over Cartesian components of the spin operators in a molecule-fixed coordinate frame. The first term corresponds to the Fermi contact interaction between the nuclear spin angular momenta, $\hat{\mathbf{I}}_i$ of the ith proton in H_2, and the spin angular momentum, $\hat{\mathbf{S}}$, of the valence electron in lithium, with $A_F^i(\mathbf{R},\mathbf{r})$ being the coupling coefficient for the Fermi contact interaction. Due to the similarity in the interaction potentials and reduced masses, the magnitude of the Fermi contact interaction in H_2–Li can be estimated from the previous work on ^{3}He–Li[53] and ^{3}He–K[54] collisions. At the zero-energy turning point of the Li–H_2 potential ($R \approx 8.75a_0$), the Fermi contact interaction constant for ^{3}He–Li[53] and ^{3}He–K[54] is on the order of 10^{-4} cm^{-1}. Since this interaction vanishes rapidly with increasing R,[54] its influence on the low-temperature Li–H_2 scattering is expected to be negligible. We thus exclude the Fermi contact interaction from our analysis. The second term in Eq. (2) is the intermolecular anisotropic hyperfine interaction, of which the strength is determined by the coupling tensor, $c^i_{\alpha\beta}(\mathbf{R},\mathbf{r})$. Since calculating the full dependence of the coupling tensor on R, θ, and r is beyond the scope of this work, we use an approximate formula that is appropriate for describing the long-range part of the anisotropic hyperfine interaction. We assume that the total nuclear spin magnetic moment of H_2, $\hat{\boldsymbol{\mu}}_{\mathrm{H_2}} = g_H\mu_N\hat{\mathbf{I}}$, and the electron spin magnetic moment of Li, $\hat{\boldsymbol{\mu}}_{\mathrm{Li}} = g_S\mu_B\hat{\mathbf{S}}$, are point dipoles located at the centers of mass of H_2 and Li, respectively. The magnetic dipole interaction between the two magnetic moments is given as[54]

$$\hat{V}_{\mathrm{SD}}(\mathbf{R},\hat{\mathbf{I}},\hat{\mathbf{S}}) = -g_S\mu_B g_{\mathrm{H}}\mu_N\sqrt{\frac{24\pi}{5}}\frac{\alpha^2}{R^3}\sum_{q=-2}^{2}(-1)^q Y_{2,-q}(\hat{\mathbf{R}})\left[\hat{\mathbf{S}}\otimes\hat{\mathbf{I}}\right]^2_q, \quad (3)$$

where g_S and g_H are the electron and proton g-factors, respectively, μ_B and μ_N denote the Bohr and nuclear magnetons, respectively, and α is the fine-structure constant. $Y_{2q}(\hat{\mathbf{R}})$ is a spherical harmonic of rank 2, which depends on the orientation of the scattering system, and $\left[\hat{\mathbf{S}}\otimes\hat{\mathbf{I}}\right]^2_q$ is a tensorial product of $\hat{\mathbf{S}}$ and $\hat{\mathbf{I}}$. We note that the general expression for the anisotropic hyperfine interactions, Eq. (2), is used in the studies of hyperfine and Zeeman effects in three-atom molecules with nonzero nuclear and electronic spins, such as HCO,[55] NH_2,[56] and Na_3.[57,58] These interactions also play a crucial role in electron spin decoherence of alkali-metal atoms trapped in solid *para*-H_2 matrices.[59] A form similar to Eq. (3) is used to describe the long-range magnetic dipolar interaction between the electron spins of $^2\Sigma$ molecules and ^2S atoms,[44,45] two $^2\Sigma$ molecules,[49] and two $^3\Sigma$ molecules.[49,60–62]

The asymptotic Hamiltonian $\hat{H}_{\mathrm{as}}$ in Eq. (1) is given by

$$\hat{H}_{\mathrm{as}} = \hat{H}_{\mathrm{H_2}} + \hat{H}_{\mathrm{Li}}, \quad (4)$$

where $\hat{H}_{\mathrm{H_2}}$ and $\hat{H}_{\mathrm{Li}}$ correspond to the Hamiltonians of the isolated molecule and atom, respectively. The effective Hamiltonian for the H_2 molecule in the ground electronic ($^1\Sigma_g^+$) state is

$$\hat{H}_{\mathrm{H_2}} = \hat{H}_{\mathrm{rot}} + \hat{H}_{\mathrm{HF}} + \hat{H}_{\mathrm{Zeeman}} \quad (5)$$

and involves the rotational, intramolecular hyperfine (HF), and Zeeman terms,

$$\hat{H}_{\mathrm{rot}} = B_v\hat{\mathbf{N}}^2 - D_v\hat{\mathbf{N}}^4, \quad (6)$$

$$\hat{H}_{\mathrm{HF}} = -c_{\mathrm{nsr}}\hat{\mathbf{N}}\cdot\hat{\mathbf{I}} + g_{\mathrm{H}}^2\mu_{\mathrm{N}}^2\left(\frac{\mu_0}{4\pi}\right)\left(\frac{\hat{\mathbf{I}}_1\cdot\hat{\mathbf{I}}_2}{r^3} - \frac{3(\hat{\mathbf{I}}_1\cdot\mathbf{r})(\hat{\mathbf{I}}_2\cdot\mathbf{r})}{r^5}\right), \quad (7)$$

$$\hat{H}_{\mathrm{Zeeman}} = -g_{\mathrm{r}}\mu_{\mathrm{N}}\hat{N}_Z B_Z - g_{\mathrm{H}}\mu_{\mathrm{N}} I_Z B_Z(1-\sigma). \quad (8)$$

Here, B_v and D_v are the effective rotational and centrifugal distortion constants in the vibrational state v. The intramolecular hyperfine Hamiltonian describes the two dominant hyperfine interactions in H_2—the nuclear spin–rotation interaction and the dipolar interaction between the nuclear spins. The respective hyperfine coupling constants, c_{nsr} and c_{dip}, quantify the strength of these two interactions. The two terms in the Zeeman Hamiltonian correspond to the contribution of the interaction of the rotational magnetic moment and the nuclear magnetic moment with the external magnetic field, with g_{r} and σ being the rotational nuclear g-factor and the anisotropic part of the nuclear shielding tensor, respectively. We assume that the external magnetic field is aligned along the space-fixed Z-axis. The diamagnetic interaction parameterized by molecular susceptibility, i.e., the interaction of the magnetic field with an induced molecular magnetic moment, contributes significantly only in intense magnetic fields ($B > 1$ T),[51] and thus, we neglect it in the following analysis.

Because our interest here is in transitions between the hyperfine states of H_2, we also neglect the internal hyperfine structure of the lithium atom. Thus, the effective Hamiltonian for the isolated lithium atom, $\hat{H}_{\mathrm{Li}}$, involves only the Zeeman term,

$$\hat{H}_{\mathrm{Li}} = -g_S\mu_B\hat{S}_Z B_Z, \quad (9)$$

where g_S is the electron spin g-factor.

The total wave function of the system is expanded in a complete set of uncoupled basis states in a space-fixed frame of Refs. 49 and 63,

$$|\Psi\rangle = \frac{1}{R}\sum_{N}\sum_{M_N=-N}^{N}\sum_{M_l=-1}^{1}\sum_{M_S=-1/2}^{1/2} \times \sum_{l}\sum_{M_l=-l}^{l} F_{NM_NM_lM_SlM_l}(R)|NM_N\rangle|IM_I\rangle|SM_S\rangle|lM_l\rangle, \quad (10)$$

where M_N, M_I, M_S, and M_l are the projections of $\hat{\mathbf{N}}$, $\hat{\mathbf{I}}$, $\hat{\mathbf{S}}$, and $\hat{\boldsymbol{l}}$ on the space-fixed Z-axis, respectively. The expansion (10) is appropriate for weakly anisotropic atom–molecule interaction potentials, such as the Li–H_2 potential used in this work.

Substitution of the total wave function from Eq. (10) to the Schrödinger equation, $\hat{H}|\Psi\rangle = E|\Psi\rangle$, leads to a set of coupled channel (CC) equations for the expansion coefficients, $F_{NM_NM_lM_SlM_l}(R)$,

$$\left[\frac{d^2}{dR^2} + 2\mu E - \frac{l(l+1)}{R^2}\right]F_{NM_NM_lM_SlM_l}(R) = 2\mu \sum_{N',M_N',M_l',M_S',l',M_l'} F_{N'M_N'M_l'M_S'l'M_l'}(R) \times \langle NM_N|\langle IM_I|\langle SM_S|\langle lM_l|\hat{V}(\mathbf{R},\mathbf{r}) + \hat{V}_{\mathrm{SD}}(\mathbf{R},\mathbf{r},\hat{\mathbf{I}},\hat{\mathbf{S}}) + \hat{H}_{\mathrm{as}}|N'M_N'\rangle|IM_I'\rangle|SM_S'\rangle|l'M_l'\rangle, \quad (11)$$

where E is the total energy and μ is defined in Eq. (1). The evaluation of the matrix elements on the right-hand side is described in Appendix A. Note that the CC equations are block-diagonal with respect to $M = M_N + M_{I_{H_2}} + M_S + M_l$, the projection of the total angular momentum, $\hat{\mathbf{J}}$, on the space-fixed Z-axis. This is a consequence of the fact that in the presence of an external magnetic field, M, contrary to J, is conserved.[49,63] This allows us to solve the CC equations for each value of M separately.

We solve the CC equations numerically (for computational details, see Sec. II A) and transform the asymptotic solution to the eigenstate basis of the asymptotic Hamiltonian (4) for H_2 in a magnetic field,

$$|(NI)\gamma_{H_2}\rangle = \sum_{M_N=-N}^{N}\sum_{M_I=-I}^{I} A^{\gamma_{H_2}}_{M_I,M_N}(B)|NM_N\rangle|IM_I\rangle, \quad (12)$$

where γ_{H_2} denotes the eigenvalue of the H_2 Hamiltonian (5). In principle, the asymptotic Hamiltonian involves a term that couples different rotational states of H_2, but this coupling is extremely small, as shown in Appendix A, so we treat N as a good quantum number. We also note that the asymptotic Hamiltonian of the Li atom, introduced in Eq. (9), is diagonal in the basis of $|SM_S\rangle$ states; thus, $|SM_S\rangle$ is an approximate eigenvector for an isolated lithium atom with $M_S = \pm 1/2$ labeling the atomic Zeeman levels. Next, we match the result to the linear combinations of the Riccati–Bessel and Neumann functions to obtain the scattering S-matrix.[64] The state-to-state cross sections are calculated from the S-matrix elements at a given collision energy, E_{kin}, by summing contributions from all M-blocks,[49]

$$\sigma_{\gamma_{H_2}M_S\to\gamma'_{H_2}M'_S}(E_{\mathrm{kin}}) = \frac{\pi}{k^2_{\gamma_{H_2}M_S}}\sum_{M}\sum_{lM_l}\sum_{l'M_{l'}}\left|\delta_{l,l'}\delta_{M_l,M_l'}\delta_{\gamma_{H_2},\gamma'_{H_2}}\delta_{M_S,M'_S} - S^{M}_{\gamma_{H_2}M_SlM_l,\gamma'_{H_2}M'_Sl'M_l'}\right|^2, \quad (13)$$

where $k_{\gamma_{H_2}M_S} = \sqrt{2\mu(E - E_{\gamma_{H_2}} - E_{M_S})}$ is the collision wavevector.

Since we are interested in the collisional relaxation of the nuclear spin states of molecular hydrogen, we define a state-to-state cross section, which is summed over the final Zeeman states of the lithium atom,

$$\sigma_{\gamma_{H_2}\to\gamma'_{H_2}}(E_{\mathrm{kin}}) = \sum_{M'_S}\sigma_{\gamma_{H_2M_S=1/2}\to\gamma'_{H_2}M'_S}(E_{\mathrm{kin}}), \quad (14)$$

and the related rate coefficient,

$$k_{\gamma_{H_2}\to\gamma'_{H_2}}(T) = \sqrt{\frac{8}{\pi\mu k_B^3T^3}}\int_0^\infty \sigma_{\gamma_{H_2}\to\gamma'_{H_2}}(E_{\mathrm{kin}})E_{\mathrm{kin}}e^{-E_{\mathrm{kin}}/k_BT}\mathrm{d}E_{\mathrm{kin}}. \quad (15)$$

In this work, we assume that the lithium atom is initially in the trappable $M_S = 1/2$ state, so we can drop the M_S symbol on the left-hand side of Eqs. (14) and (15).

When considering collisions in the absence of an external magnetic field, we expand the total wave function as follows:

$$|\Psi\rangle = \frac{1}{R}\sum_{N}\sum_{F=|N-1|}^{N+1}\sum_{M_S=-1/2}^{1/2}\sum_{l}\sum_{M_l=-l}^{l} F_{NFM_FM_SlM_l}(R) \times |(NI)FM_F\rangle|SM_S\rangle|lM_l\rangle, \quad (16)$$

i.e., we use the coupled basis vectors to represent the states of H_2,

$$|(NI)FM_F\rangle = (-1)^{-N+1-M_F}\sum_{M_N=-N}^{N}\sum_{M_I=-1}^{1}\sqrt{2F+1} \times \begin{pmatrix} N & 1 & F \\ M_N & M_I & -M_F \end{pmatrix}|NM_N\rangle|IM_I\rangle. \quad (17)$$

Here, $\begin{pmatrix} \cdot & \cdot & \cdot \\ \cdot & \cdot & \cdot \end{pmatrix}$ are the 3-j symbols[65] and $F = |\hat{\mathbf{F}}|$ is the quantum number associated with the total angular momentum of H_2, in which $\hat{\mathbf{F}}$ is the result of coupling of $\hat{\mathbf{N}}$ to $\hat{\mathbf{I}}$. This representation is convenient because F is conserved in the field-free case; see Sec. III. The rest of the procedure follows the same steps as detailed above and hence is not repeated here. The matrix elements of the PES, the spin-dependent interaction, and the asymptotic Hamiltonian in the coupled basis [see Eq. (16)] are provided in Appendix B.

A. Computational details

The spectroscopic constants used to parameterize the Hamiltonian of H_2 [Eq. (5)] and Li [Eq. (9)] are listed in Table I. We use the *ab initio* H_2–Li PES reported by Makrides *et al.*[48] This PES has recently been used in the calculations of elastic, inelastic, and glancing-angle rate coefficients for collisions of ultracold Li atoms with room-temperature H_2 molecules in the context of the calibration of a cold-atom vacuum standard.[48,70–72] For the purpose of solving the CC equations, we expand the PES in Legendre polynomials [Eq. (A1)]. Since H_2 is a homonuclear molecule, the expansion index takes only even values. We truncate the expansion in Eq. (A1) at $\lambda_{\max} = 4$. The dependence of the expansion coefficients on the H_2 stretching coordinate, r, is averaged out by the integration over rovibrational wave functions of the isolated H_2 molecule in the ground vibrational state; see Eq. (A3) for details.

TABLE I. Spectroscopic parameters of H_2 used in the calculations reported in the present work.

Constant	Value	Source
B_v	59.322 cm^{-1}	66
D_v	4.575×10^{-2} cm^{-1}	66
c_{nsr}	$(3.81 \pm 0.01) \times 10^{-6}$ cm^{-1}	27
c_{dip}	$(9.614 \pm 0.005) \times 10^{-6}$ cm^{-1}	27
g_r	0.882 5	67
g_H	5.585 694 698 3	68
σ	1.76 ppm	69

We solve the CC equations using a log-derivative propagator[64,73] on a radial grid from $R_{min} = 3.0a_0$ to $R_{max} = 200a_0$ (for collisions with $E_{kin} < 10^{-2}$ cm^{-1}, we increase R_{max} to $500a_0$) with a constant step size of $0.05a_0$. While this integration range is notably smaller than that used in Ref. 48, where the authors extended R_{max} to $5000a_0$, we validated that it is sufficient to ensure a subpercent convergence of the state-to-state cross sections. We cover the range of kinetic energies from 10^{-9} to 50 cm^{-1}. Due to the weak anisotropy of the Li–H_2 PES, it is sufficient to keep only the lowest two rotational levels of *ortho*-H_2 ($N = 1$ and $N = 3$) in the basis to obtain a subpercent convergence of the cross sections. The number of partial waves, l_{max}, included in our calculations depends on the collision energy and varies from 6 up to 55. To verify our calculations, we compared the field-free cross sections with the previous results[48] and found excellent agreement. Finally, we note that the exact value of the rotational constant has no significant influence on the cross sections. For instance, switching between $B_{v=0}$ and B_e modifies the elastic cross section for the scattering of H_2 in the $F = 0$ hyperfine state by 0.03% and the inelastic cross sections by less than 0.005%.

III. RESULTS: FIELD-FREE H_2–Li COLLISIONS

In the absence of an external magnetic field, the $v = 0, N = 1$ state of H_2 is split into three hyperfine levels, spread over a range of ~600 kHz,[27] as shown in the inset of Fig. 1(a). The three states are labeled by F, the total angular momentum of H_2. We present the hyperfine-resolved state-to-state cross sections of H_2 ($v = 0, N = 1$) colliding with ^{6}Li in Fig. 1. The elastic (F-conserving) cross sections are shown in Fig. 1(a) as blue ($F = 2$), green ($F = 1$), and red ($F = 0$) lines. The cross sections are almost identical, apart from kinetic energies close to the feature located at $E_{kin} = 1.2$ cm^{-1}, where the largest difference between the cross sections approaches 20%. This structure was attributed to the g-wave ($l = 4$) shape resonance in Ref. 48. The inelastic (F-changing) cross sections are typically orders of magnitude smaller than the elastic cross sections. However, near $E_{kin} = 1.2$ cm^{-1}, this difference narrows to a factor of 2.5. The three panels [(b)–(d)] provide additional information

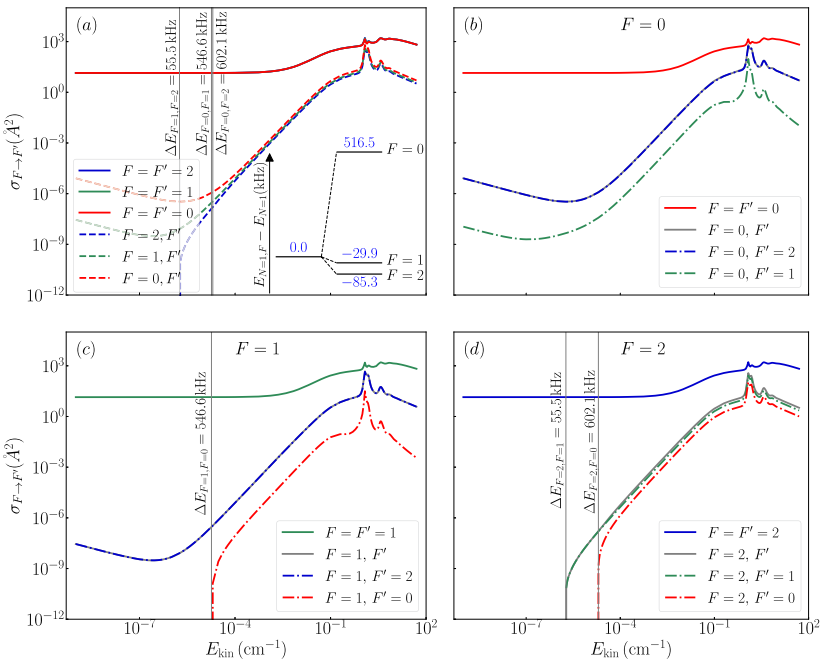

FIG. 1. Hyperfine-resolved state-to-state cross sections for collisions of H_2 with ^{6}Li. Panel (a) presents the elastic (F-conserving) cross sections (solid lines) and the total inelastic state-to-state cross sections (dashed lines) for a given F initial state. The gray vertical lines correspond to the energy differences between the three hyperfine states and are shown to illustrate the mechanism of channel opening. The energy diagram in the bottom right corner of panel (a) shows the hyperfine structure of the $v = 0, N = 1$ level of H_2. In panels (b)–(d), we show the cross sections separately for each initial value of F along with the decomposition of the total inelastic cross section into the different final state, F', contributions.

about the inelastic processes that affect each F-labeled state. Inelastic scattering from the $F = 0$ state, which has the largest energy, is dominated by the $F = 0 \rightarrow F' = 2$ de-excitation [the grey solid and blue dotted-dashed lines in Fig. 1(b) are almost overlapped]. This process is driven by the $\lambda = 2$ anisotropic term of the Li–H_2 PES [see Eq. (B1)]. The $F' = 1$ state is not directly coupled to the initial state by the PES (there is no $\lambda = 1$ term in the PES expansion since H_2 is a homonuclear molecule), and the cross sections for the $F = 0 \rightarrow F' = 1$ de-excitation are at least one order of magnitude smaller than those for the $F = 0 \rightarrow F' = 2$ transition. The nuclear spin–electron spin interaction introduces a weak coupling between the $F = 0$ and $F = 1$ levels, which influences the cross sections only for kinetic energies smaller than 10^{-6} cm^{-1} as discussed below. Similarly, inelastic scattering from the $F = 1$ state is dominated by the $F = 1 \rightarrow F' = 2$ de-excitation, driven by the $\lambda = 2$ term in the PES expansion. When the kinetic energy crosses the $\Delta E_{F=0,F=1} = E_{F=0} - E_{F=1}$ threshold (at 546.5 kHz), the excitation to the $F = 0$ state becomes energetically accessible. As mentioned above, since the $F = 1$ and $F = 0$ channels are not directly coupled by the PES, this contribution to the total inelastic cross section is significantly (two orders of magnitude) weaker than the $F = 1 \rightarrow F' = 2$ de-excitation. For the $F = 2$ initial state, we note that until the kinetic energy surpasses the first threshold ($E_{F=1,F=2} = E_{F=1} - E_{F=2}$ at 54.6 kHz), the scattering is purely F-conserving. Both the $F = 2 \rightarrow F' = 1$ and $F = 2 \rightarrow F' = 0$ excitations are driven by the $\lambda = 2$ term (with a weak contribution from the spin-dependent interaction).

Overall, the magnetic dipole–dipole interaction, Eq. (3), has a negligible influence on the state-to-state cross sections for collisions of H_2 with ^{6}Li in the absence of an external magnetic field. The only significant effect that we observe is an enhancement of the $\Delta F = 1$ de-excitation in the ultracold regime (below 10^{-6} cm^{-1})—the dashed and solid lines in Fig. 2 represent the values of $\sigma_{F\rightarrow F'=F+1}$ calculated with and without the spin-dependent H_2–Li interaction, respectively. Interestingly, the inclusion of this weak interaction is necessary to obtain the Wigner threshold behavior[74] of the $\sigma_{F=0\rightarrow F'=1}$ cross section ($\sigma \sim E_{\rm kin}^{-1/2}$) at $E_{\rm kin} \approx 10^{-6}$ cm^{-1}. We observe a slight alternation of the $\Delta F = -1$ *excitation* cross sections near the thresholds ($\Delta E_{F=0,F=1} = 546.5$ kHz and $E_{F=1,F=2} = 54.6$ kHz), which is not shown in Fig. 2. In the remaining field-free cases (larger relative kinetic energies and other scattering processes), the nuclear spin–electron spin interaction has a negligible influence on the state-to-state cross sections.

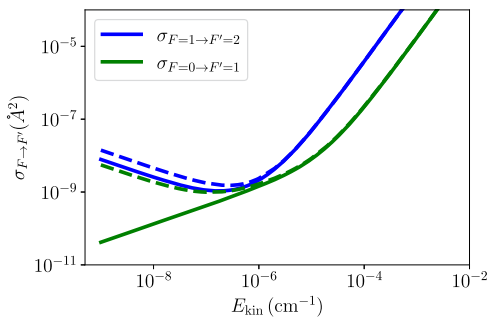

FIG. 2. Influence of the nuclear spin–electron spin interaction on the hyperfine-structure resolved state-to-state cross sections for collisions of H_2 with ^{6}Li. The dashed and solid lines present the cross sections calculated including and neglecting the spin-dependent interaction, respectively.

IV. RESULTS: H_2–Li COLLISIONS IN AN EXTERNAL MAGNETIC FIELD

Before proceeding to discuss the results of scattering calculations, we briefly consider the energy structure of the H_2 molecule in an external magnetic field. Figure 3(a) shows the Zeeman energy levels in the $v = 0, N = 1$ rovibrational manifold of *ortho*-H_2 obtained by diagonalization of the Hamiltonian in Eq. (5) with the spectroscopic parameters of H_2 gathered in Table I. At large field strengths, the nine levels are grouped into sets of three states, which share the same projection of the nuclear spin, M_I. This reflects the relative strength of the nuclear Zeeman term with respect to the rotational Zeeman term—for $N = 1$, the first term in Eq. (8) is approximately six times smaller than the second term. Within each group of states, the order of states (starting from states with the largest energy) is $M_N = -1, 0$, and 1. At high fields, the top three low-field-seeking Zeeman states, which are amenable to magnetic trapping, correspond to $M_I = -1$.

While we use the M_I and M_N quantum numbers to describe the Zeeman states at high fields, it is important to acknowledge that at lower fields, the eigenstates undergo significant mixing due to the nuclear spin–rotation and nuclear spin–nuclear spin interactions. This situation requires us to use a more general approach for labeling and referencing the Zeeman states throughout the entire range of magnetic fields. To this end, we introduce a "state index" (SI) that uniquely identifies each eigenstate, ranging from 1 to 9, as shown in Fig. 3(a). The three trappable states thus have SI = 1, 2, and 3.

We perform quantum scattering calculations at magnetic field strengths ranging from 10^{-4} to 1 T. As an example, we discuss the kinetic energy dependence of the state-to-state cross sections for H_2–Li collisions at $B = 0.3$ T, which corresponds to a magnetic trap depth of ~0.8 mK for the SI = 1 state. We consider the collisions of H_2 and Li in their low-field seeking states (SI = 1, 2, and 3 for H_2 and $M_S = 1/2$ for Li, respectively). Panels (b)–(d) in Fig. 3 show the cross sections for elastic and all inelastic transitions in H_2–Li collisions at $B = 0.3$ T. The color of each curve matches that of the corresponding Zeeman level plotted in Fig. 3(a).

The elastic cross sections are consistently larger than the total inelastic cross sections by at least two orders of magnitude, except in the vicinity of $E_{\rm kin} = 1.2$ cm^{-1}, where γ decreases to ~3. For the sake of discussion, we distinguish two specific regimes, namely, the ultralow collision energy regime ($E_{\rm kin} < 10^{-5}$ cm^{-1}), the low collision energy regime ($E_{\rm kin} > 10^{-2}$ cm^{-1}), and an intermediate regime.

A. Ultralow collision energy regime

At ultralow collision energies, inelastic cross sections follow the $\sim E_{\rm kin}^{-1/2}$ behavior predicted by Wigner's threshold law.[74] For the low-field-seeking state with the largest internal energy [SI = 1, panel (b) in Fig. 3], two key events contribute to the total inelastic cross section. The first is the $\Delta M_I = \Delta M_N = 0, \Delta M_S = -1$ transition, i.e., the relaxation of lithium's electron spin, with H_2 remaining in the same Zeeman state. Although this process clearly does not lead to the transition of H_2 to an untrappable state, it involves the release of a

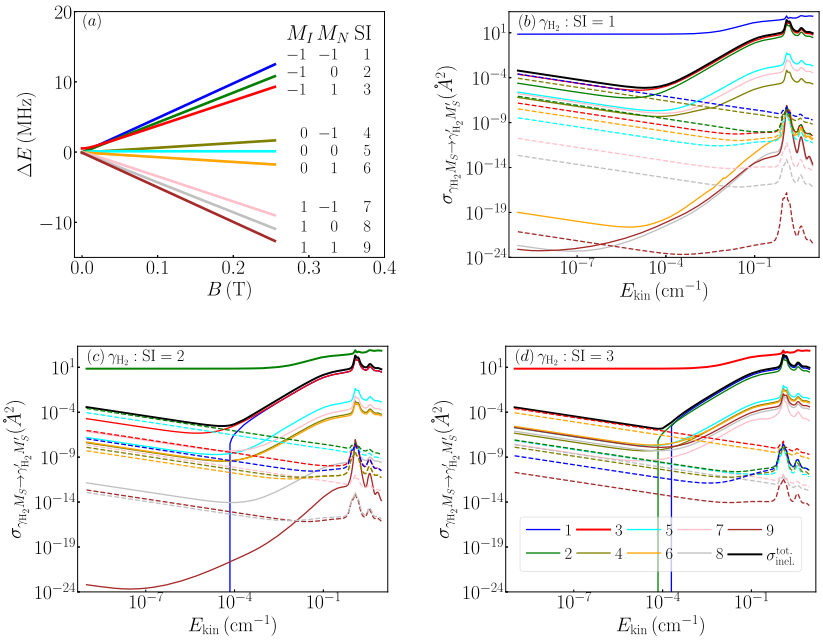

FIG. 3. Panel (a): Zeeman sublevels of the $v = 0, N = 1$ rovibrational state of H_2 as a function of magnetic field B. Panels (b)–(d): Cross sections for H_2–Li collisions in an external magnetic field $B = 0.3$ T. The three panels correspond to different initial levels of H_2: the first [panel (b)], second [panel (c)], and third states [panel (d)], according to the state labels in panel (a). The solid lines correspond to the collisional events, in which the electron spin of ^{6}Li is conserved, and the dashed lines correspond to those, in which the electron spin is flipped ($M_S = 1/2 \to M'_S = -1/2$).

large amount of energy ($g_S\mu_B B_Z \approx 0.4$ K), which will induce H_2 loss. The second is a nuclear-spin-conserving $\Delta M_I = 0$, $\Delta M_N = 2$ transition ($\Delta M_S = 0$, see the solid red curve). While this process leads to the loss of H_2 population from the SI = 1 state, the molecule remains in one of the low-field seeking states after the collision. The process releases ~0.1 mK of energy. The third most prominent contribution, albeit smaller by a factor of 2.5, is the spin–exchange collision that involves a simultaneous change in the nuclear spin of H_2, $\Delta M_I = +1$, and relaxation of lithium's electron spin, $\Delta M_S = -1$, while conserving the projection of rotational angular momentum, $\Delta M_N = 0$; see the olive dashed curve in Fig. 3(b). Note that this process is driven directly by the spin-dependent H_2–Li interaction [Eq. (3)].

For the second low-field-seeking initial state of H_2 [SI = 2, panel (c) in Fig. 3], the two most significant contributions to the total inelastic cross sections stem from lithium's spin-flipping transitions ($\Delta M_S = -1$), with either no change of the H_2 quantum numbers ($\Delta M_I = \Delta M_N = 0$) or a simultaneous change of $\Delta M_I = +1$ (with $\Delta M_N = 0$); see the green and blue dashed lines in Fig. 3(c), respectively. While the first transition is essentially elastic for H_2, it releases an energy of $g_S\mu_B B_Z \approx 0.4$ K. The second one is another example of nuclear spin–electron spin exchange driven by the spin-dependent interaction [Eq. (3)]. In both cases, the released energy will remove the H_2 molecule from the magnetic trap. The third most important contribution (four-times smaller than the nuclear spin–electron spin exchange) comes from a nuclear spin-conserving ($\Delta M_I = 0$) relaxation to the SI = 3 state (with $\Delta M_N = +1$), with no change in lithium's electron spin ($\Delta M_S = 0$). Note that the transition to the SI = 1 low-field-seeking state of H_2 is only energetically accessible through a simultaneous spin-flip of lithium and provides a negligible (10^{-3}) contribution to the total inelastic cross section.

For the third low-field-seeking initial state of H_2 [SI = 3, panel (d) in Fig. 3], two processes make up 99% of the total inelastic cross section. The first process conserves the Zeeman state of H_2 ($\Delta M_N = \Delta M_I = 0$) but involves a spin flip ($\Delta M_S = -1$) accompanied by an energy release. The second process is a nuclear spin–electron spin exchange ($\Delta M_S = -1, \Delta M_I = +1$), which conserves M_N. Note that M_I-conserving transitions that do not involve a simultaneous spin flip in lithium are not energetically accessible at $E_{\text{kin}} \lesssim 10^{-4}$ cm^{-1}.

In all three cases discussed so far, although the M_I, M_N, or M_S-changing processes lead to undesirable energy release and loss of H_2 population from the trap, the cross sections for these processes are over four orders of magnitude smaller than the elastic cross section at collision energies below 10^{-5} cm^{-1}. This suggests excellent prospects for sympathetic cooling of H_2 in the low-field-seeking states (SI = 1–3) via collisions with spin-polarized Li atoms in a magnetic trap.

B. Low collision energy regime

The second regime involves kinetic energies larger than 10^{-2} cm^{-1}. Interestingly, for all three initial low-field-seeking states of H_2, the cross sections fall into three distinct categories. The dominant contribution (at the level of 99.9%) to the inelastic cross section always comes from M_I-conserving transitions. The second category provides the contribution at the level of 10^{-3}–10^{-5}. For the

SI = 1 low-field-seeking state [panel (b) in Fig. 3], the second category involves two transitions that alter M_I by +1 and either conserve M_N or change M_N by +1 and one $\Delta M_I = +2$, $\Delta M_N = 0$ transition. For the SI = 2 low-field-seeking state [panel (c) in Fig. 3], the second category involves three $\Delta M_I = +1$ transitions (with $\Delta M_N = -1, 0, 1$) and one $\Delta M_I = +2$, $\Delta M_N = -1$ transition. Finally, the second category for the SI = 3 trappable state [panel (d) in Fig. 3] involves all $\Delta M_I = +1, +2$ transitions. In all three cases, the third group encompasses all transitions, which affect the electronic spin of lithium ($\Delta M_S = -1$). It additionally involves the two M_S-conserving transitions with $\Delta M_I = +2$ for the SI = 1 ($1 \to 8$ and $1 \to 9$) and SI = 2 ($2 \to 8$ and $2 \to 9$) low-field-seeking states and a $\Delta M_I = +1$, $\Delta M_N = +2$ transition from the SI = 1 state ($1 \to 6$).

Our results indicate a clear tendency in favor of M_I- and M_S-conserving transitions in an external magnetic field. Similar propensity rules were observed for M_S in cold collisions of ^{40}CaH($X^2\Sigma^+, v = 0, N = 1, M_N = 1, M_S = 1/2$) molecules with ^{4}He[75] and for M_I in collisions of ^{13}CO ($X^1\Sigma^+, v = 0, N = 1$) with ^{4}He.[51] The strong suppression of M_I- and M_S-changing collisions in the external magnetic field can be compared to the electron and nuclear spin selection rules in spectroscopy, $\Delta S = 0$, and $\Delta I = 0$.[76]

An intriguing feature of the H_2–Li system is the presence of $\Delta M_I = 2$ transitions in the second category (or "group-II" transitions, as defined in Ref. 51). In the case of transitions from the SI = 1 and 2 states, it is the $\Delta M_I = 2$ transition to the SI = 7 state. Its relative strength can be attributed to a slight contribution of the $|N = 1, M_N = 1\rangle|I = 1, M_I = -1\rangle$ bare state to the SI = 7 state. The mixing of the $|N = 1, M_N = 1\rangle|I = 1, M_I = -1\rangle$ and $|N = 1, M_N = -1\rangle|I = 1, M_I = 1\rangle$ basis states is driven by the nuclear spin–spin interactions between the two protons of the H_2 molecule [Eq. (A7)]. We performed additional calculations, where we excluded the intramolecular nuclear spin–nuclear spin interaction from the asymptotic Hamiltonian [Eq. (5)], and we found that the cross sections for $\Delta M_I = 2$ transitions decreased by four orders of magnitude. Note that this interaction is absent in the ^{13}CO molecule, studied in Ref. 51.

C. Magnetic field dependence of the cross sections

Here, we discuss the magnetic field dependence of the state-to-state cross sections across three distinct collision energy regimes: ultra-low (10^{-6} cm^{-1}), intermediate (10^{-4} cm^{-1}), and low (1 cm^{-1}). The discussion builds on the results in Sec. IV B, as we focus on collisions of H_2 in the three magnetically trappable states, SI = 1, 2, and 3, as shown in Fig. 4. In all panels, the color of each curve corresponds directly to the color of the respective final Zeeman level (see Fig. 3).

We observe that the elastic cross sections are field-independent and by far exceed the inelastic cross sections. The dependence of the inelastic cross sections on B varies with the kinetic energy and the final Zeeman state. For instance, in the ultra-low energy regime [panels (a)–(c) in Fig. 4], we observe a systematic increase in the values of the cross sections with B. However, two distinct deviations from this pattern emerge. The first one is related to the observed resonance-like features at 0.0025 and 0.5 T for the final Zeeman states with SI = 7 and 5, respectively [see the pink and light blue curves in panels (a), (b), (d), (e), (g), and (h) in Fig. 4]. These will be discussed further in the next paragraph. The other exception is the sharp decline for excitation transitions, such as SI = $2 \to 1$ at 0.008 T [the blue curve in panel (b)]. This is due to the closure of inelastic channels due to increasing spacing between the initial and final Zeeman sublevels with increasing magnetic field. The sharp increase in the cross sections [see, for instance, the orange, light blue, and red curves in panel (a)] corresponds to the opening of the additional inelastic channels. As the kinetic energy increases [see panels (d)–(f)], more channels become energetically accessible, even at low B field values. Meanwhile, the fields at which some of the inelastic channels become inaccessible are shifted toward larger values. Finally, in the low energy regime [panels (g)–(i)], we can categorize inelastic cross sections into two main classes. The cross sections

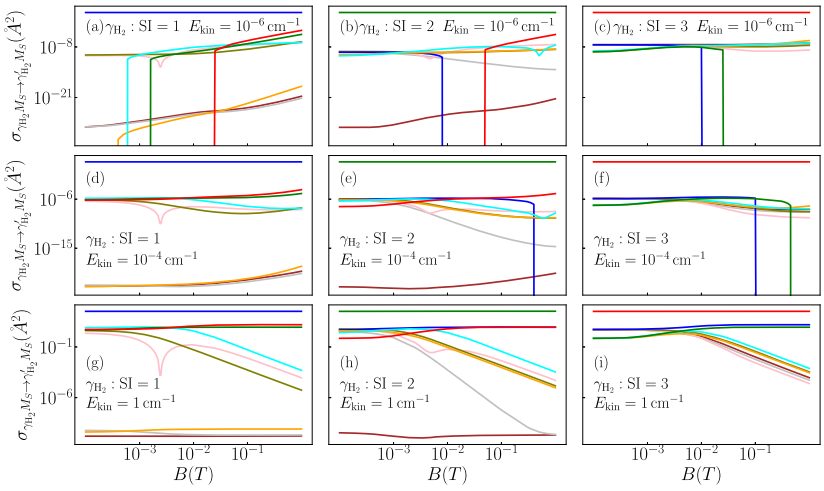

FIG. 4. State-to-state cross sections for cold H_2–Li collisions in the three Zeeman states amenable to magnetic trapping (γ_{H_2} : SI = 1, 2, and 3), as a function of the external magnetic field, B. The initial and final states of the lithium atom are fixed to $M_S = 1/2$. The final Zeeman states in each panel are color-coded according to Fig. 3.

from the first class exhibit a negligible field dependence. The cross sections from the second class are field-independent at low B values but decrease monotonically with increasing B for fields larger than 10^{-2} T. We explain this behavior in detail below, focusing on the case of the scattering from the SI = 1 state [panel (g)].

As discussed in Sec. IV B, we observe a clear propensity for $\Delta M_I = 0$ transitions. This propensity rule is evident here too, as emphasized by the green and red curves across the considered field ranges: the cross sections for transitions to the SI = 2 and 3 states are notably larger than others. Furthermore, they exhibit a weak field dependence. Transitions to the weakly coupled ($\Delta M_I = 2$) SI = 8 and 9 states [grey and dark red lines in panel (g)] are orders of magnitude smaller. Interestingly, they are also field-independent, suggesting that the lack of strong coupling makes them less susceptible to the variations in B. Apart from these two cases, the same observation holds for the transition to the SI = 6 state (orange curve): the relative weakness of this cross section is related to the admixture of the $|N = 1, M_N = 0\rangle|I = 1, M_I = 1\rangle$ basis state. A completely different behavior of the cross sections as a function of B is observed for three other final Zeeman states. The transition to the SI = 4 state (olive line) is one of the most important inelastic processes at low values of B. This is because of the admixture of the $|N = 1, M_N = -1\rangle|I = 1, M_I = 0\rangle$ state through the nuclear spin–rotation interaction. As the field increases, so does the energy spacing between the two states, and the mixing becomes less significant. The pronounced magnetic-field dependence of the cross sections to the Zeeman eigenstates composed of strongly mixed bare states $|NM_N\rangle|IM_I\rangle$ was observed in Ref. 51 for the $^{13}C^{16}O$–He system and explained in the framework of the Born approximation. For the transitions to the SI = 5 and 7 states (denoted by the light blue and pink lines), the dynamics are influenced by the fact that they are composed of three strongly mixed bare states $|NM_N\rangle|IM_I\rangle$ with $M_N + M_I = 0$. This mixing stems from the interplay of the nuclear spin–rotation and nuclear spin–nuclear spin interactions (the three states constitute a 3×3 matrix of states with $M_F = 0$). The mixing becomes less pronounced as the field increases, although there exists a resonant-like feature at 0.002 45 T for the SI = 1 → SI = 7 transition. We note that this feature is independent of the relative kinetic energy of the collision. The nature of this resonant-like feature and the potential for identifying such resonances in other systems will be explored in a forthcoming publication.

We note similar patterns for inelastic collisions originating from the SI = 2 and 3 states. The majority of significant inelastic processes favor the $\Delta M_I = 0$ propensity rule, showing only minor variations with increasing fields. For the SI = 2 state, five distinct transitions exhibit a linear decrease with the field. This pattern traces back to the admixture of the $|N = 1, M_N = 1\rangle|I = 1, M_I = -1\rangle$ basis state, primarily responsible for the elevated magnitudes of the inelastic cross sections at lower fields. As B increases, the mixing becomes less pronounced, leading to the decreasing magnitude of the cross sections at higher B values. Finally, the SI = 3 state is somewhat special: 6 out of 9 cross sections exhibit a systematic decrease with the field. All of these are "group-II" transitions identified in Sec. IV B. Their decrease with increasing B can be understood by the decreasing admixture of the $|N = 1, M_N = 1\rangle|I = 1, M_I = -1\rangle$ bare state to the SI = 5 and 7 states (light blue and pink curves, respectively), the decreasing admixture of the $|N = 1, M_N = 0\rangle|I = 1, M_I = -1\rangle$ bare state to the SI = 4 state (olive curve), or the increasing energy separation from the rest of the Zeeman states.

D. Elastic-to-inelastic scattering ratio

Here, we explore the potential of atomic lithium as a sympathetic coolant for the H_2 molecule. While the mismatch between Zeeman splittings of H_2 and ^{6}Li presents a challenge for the experimental realization of a two-species trap, here, we focus on estimating the efficiency of the cooling mechanism. Specifically, we determine the elastic-to-inelastic ratio and estimate the optimal lithium density that yields the most effective thermalization during collisions.

To this end, we calculate the average state-to-state cross sections for Li–H_2 collisions for the three initial trappable states (SI = 1, 2, and 3) of H_2 [see Eq. (14)] and the corresponding rate coefficients k, given by Eq. (15). Note that the initial state of lithium is fixed to the trappable $M_S = 1/2$ state.

The rate coefficients are presented in Fig. 5. The elastic scattering rates for the three trappable states of H_2 are nearly identical to the corresponding rate coefficients calculated without the hyperfine structure and external magnetic field, $k^{\text{el.}}_{N=1}$ (black solid line in Fig. 5). The largest difference between $k^{\text{el.}}_{N=1}$ and $k^{\text{el.}}_{\gamma_{H_2}}$ is ~3%. The solid lines in Fig. 5 correspond to the total inelastic rate coefficients. To check whether the sympathetic cooling of H_2 by ^{6}Li is feasible, we plot in Fig. 5 the elastic rate coefficient multiplied by $\frac{1}{100}$ (efficient cooling requires $k^{\text{el.}}/k^{\text{inel.}} \geq 100$). At first sight, it seems that this condition is fulfilled for temperatures below 50 mK. We recall that the proposed trap depth is ~0.8 mK for the SI = 1 state of H_2. However, the total inelastic cross section is dominated by transitions to other trappable states (transitions with $\Delta M_I = 0$). Thus, the rate of inelastic scattering to states that are *not* amenable to magnetic trapping is several orders of magnitude lower (see the dashed lines in Fig. 5), and the corresponding elastic-to-inelastic scattering ratio is always larger than 10^4. Transitions to other trappable states release energy (~10 times lower than the trap depth), which could result in heating, but not trap loss, being of minor concern for sympathetic cooling experiments.

We also estimate the rate of thermalizing collisions (in s^{-1}) as

$$R = k^{\text{el.}}_{\gamma_{H_2}} n_0. \tag{18}$$

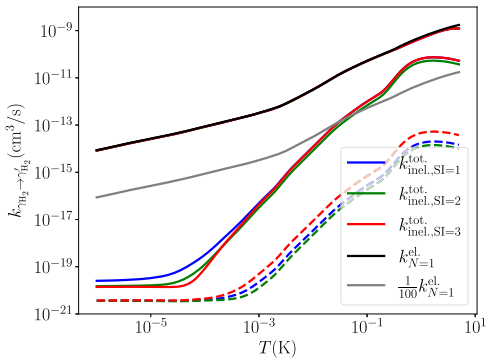

FIG. 5. Rate coefficients for elastic and inelastic transitions in Li–H_2 collisions for the three trappable Zeeman sublevels of H_2 ($v = 0, N = 1$) at 0.3 T. The elastic rates are almost identical to the field- and hyperfine-free elastic rate coefficients for the $v = 0, N = 1$ state (black solid line). The total inelastic rate coefficients and the inelastic rate coefficients to the untrappable states are presented as solid and dashed lines, respectively. The gray solid line presents the elastic rate coefficient multiplied by $\frac{1}{100}$.

Taking the elastic rate coefficient for the SI = 1 state of H_2 at 1 mK (3.2×10^{-13} cm^3 s^{-1}) and the density of ^{6}Li atoms in the UV MOT[47] operating at 59 μK ($n_0 = 2.9 \times 10^{10}$ cm^{-3}), we obtain $R \approx 10^{-2}$ s^{-1}. For efficient sympathetic cooling, the rate of thermalizing collisions should be higher by at least two orders of magnitude. This can be achieved by increasing the density of the lithium MOT, either by using higher magnetic field gradients or larger detunings of the UV light. The increased density is then achieved with a trade-off for an increased temperature of the Li atoms.

V. CONCLUSIONS

We performed a rigorous quantum dynamical analysis of the effects of hyperfine and Zeeman interactions on cold and ultracold atom–H_2 collisions. We investigated the cold collisions of molecular hydrogen in the $v = 0, N = 1$ rovibrational state with ^{6}Li atoms using CC quantum scattering calculations based on an accurate *ab initio* PES. In the field-free case, we found that the three hyperfine levels of the $v = 0, N = 1$ state in H_2 predominantly undergo elastic collisions. The magnetic dipolar interaction between the electronic spin in lithium and the total nuclear spin of H_2 exerts a pronounced inference on ultracold Li–H_2 collisions, enhancing the $F = 0 \rightarrow F' = 1$ transitions.

We found that the collisional dynamics of H_2 in low-field-seeking states in the presence of an external magnetic field is dominated by elastic, rather than inelastic, collisions. Inelastic collisions tend to conserve the space-fixed projection of the nuclear spin in H_2. The magnetic dipolar interaction between the nuclear spin of H_2 and the electronic spin of Li drives the electron spin relaxation and the nuclear spin–electron spin exchange, two key inelastic processes in the ultracold regime.

Finally, we discussed the results in the context of the experimental realization of sympathetic cooling of H_2 by ultracold spin-polarized Li atoms. Given the predominance of elastic collisions and the propensity of inelastic scattering to retain H_2 in its low-field-seeking states, the elastic-to-inelastic collision ratio for Li–H_2 is favorable for sympathetic cooling ($\gamma > 100$). However, to realize efficient sympathetic cooling, the current densities of Li in a MOT must be increased by at least two orders of magnitude.

ACKNOWLEDGMENTS

This research was funded by the European Union (Grant Nos. ERC-2022-STG, H2TRAP, and 101075678). Views and opinions expressed are, however, those of the author(s) only and do not necessarily reflect those of the European Union or the European Research Council Executive Agency. Neither the European Union nor the granting authority can be held responsible for them. H.J. is supported by the Foundation for Polish Science (FNP). T.V.T. acknowledges the support from the NSF CAREER Award No. PHY-2045681. This research was financed from the budgetary funds on science projected for 2019–2023 as a research project under the "Diamentowy Grant" program. We gratefully acknowledge Polish high-performance computing infrastructure PLGrid (HPC Centers: ACK Cyfronet AGH, CI TASK) for providing computer facilities and support within computational Grant No. PLG/2023/016279. Calculations have been carried out using resources provided by Wroclaw Centre for Networking and Supercomputing (http://wcss.pl), Grant No. 546. This research is part of the program of the National Laboratory FAMO in Toruń, Poland.

AUTHOR DECLARATIONS

Conflict of Interest

The authors have no conflicts to disclose.

Author Contributions

Hubert Jóźwiak: Conceptualization (equal); Funding acquisition (supporting); Investigation (lead); Methodology (equal); Software (equal); Visualization (lead); Writing – original draft (lead). **Timur V. Tscherbul**: Conceptualization (equal); Funding acquisition (supporting); Methodology (equal); Resources (supporting); Software (equal); Supervision (supporting); Validation (lead); Writing – review & editing (equal). **Piotr Wcisło**: Conceptualization (equal); Funding acquisition (lead); Resources (lead); Supervision (lead); Validation (supporting); Writing – review & editing (equal).

DATA AVAILABILITY

The data that support the findings of this study are available from the corresponding author upon reasonable request.

APPENDIX A: MATRIX ELEMENTS IN EQ. (11)—THE UNCOUPLED BASIS

Here, we present a derivation of the matrix elements that enter the CC equations [Eq. (11)]. Following the standard approach,[49] we expand the H_2–Li interaction potential in Legendre polynomials,

$$V(\mathbf{R}, \mathbf{r}) = \sum_{\lambda=0}^{\lambda_{\max}} V_\lambda(R, r) P_\lambda(\cos\theta). \tag{A1}$$

Since H_2 is a homonuclear molecule, λ takes only even values. We truncate the expansion at $\lambda_{\max} = 4$. The interaction potential is diagonal in all spin projections (M_I, M_S, and $M_{I_{\mathrm{Li}}}$) with matrix elements,[49]

$$\begin{aligned}
&\langle NM_N|\langle IM_I|\langle SM_S|\langle lM_l|\hat{V}(\mathbf{R},\mathbf{r})|N'M_N'\rangle|IM_I'\rangle|SM_S'\rangle|l'M_l'\rangle \\
&= \delta_{M_S M_S'}\delta_{M_I M_I'}(-1)^{M_l'-M_N}\sqrt{[N,N',l,l']}\sum_{\lambda=0}^{\lambda_{\max}} v_{\lambda,v=0}^{N,N'}(R)\begin{pmatrix} l & \lambda & l' \\ 0 & 0 & 0 \end{pmatrix} \\
&\times \begin{pmatrix} l & \lambda & l' \\ -M_l & \Delta M_l & M_l' \end{pmatrix}\begin{pmatrix} N & \lambda & N' \\ 0 & 0 & 0 \end{pmatrix}\begin{pmatrix} N & \lambda & N' \\ -M_N & \Delta M_N & M_N' \end{pmatrix}.
\end{aligned} \tag{A2}$$

Here, $\Delta M_x = M_x - M_x'$ for all angular momentum projections ($x = l, N, S, I$) and $[x_1, x_2, \ldots, x_N] = (2x_1 + 1)(2x_2 + 1)\ldots(2x_N + 1)$. We note that the interaction potential mixes states with different M_l and M_N. At the same time, the interaction conserves the sum $M_l + M_N$ and, as a result, the projection of the total angular momentum, M. The coefficients $v_{\lambda,v=0}^{N,N'}(R)$ are obtained by taking the matrix elements of the Legendre moments in Eq. (A1), $V_\lambda(R, r)$, between the rovibrational wave functions of the H_2 molecule in the $v = 0$ state,

$$v_{\lambda,v=0}^{N,N'}(R) = \int_0^\infty \mathrm{d}r \chi_{v=0,N}(r) V_\lambda(R, r) \chi_{v=0,N'}(r). \tag{A3}$$

Rovibrational wave functions of H_2, $\chi_{v,N}$, are obtained by solving the Schrödinger equation for the nuclear motion of H_2 with the potential energy curve of Schwenke[77] using the discrete variable representation–finite basis representation method. Due to a weak dependence of the $v^{N,N'}_{\lambda,v=0}(R)$ terms on N, we use $N = N' = 1$ in scattering calculations.

The magnetic dipolar interaction between the nuclear spin of H_2 and the electron spin of Li [see Eq. (3)] is diagonal in N and M_N,

$$\begin{aligned}
&\langle NM_N|\langle IM_I|\langle SM_S|\langle lM_l|\hat{V}_{\mathrm{SD}}(\mathbf{R},\mathbf{r},\hat{\mathbf{I}},\hat{\mathbf{S}})|N'M'_N\rangle|IM'_I\rangle|SM'_S\rangle|l'M'_l\rangle \\
&\quad = -\delta_{NN'}\delta_{M_NM'_N} g_S\mu_B g_{\mathrm{H}}\mu_N \left(\frac{\alpha^2}{R^3}\right)\sqrt{30}(-1)^{-M_l+I-M_{\mathrm{H}_2}+S-M_S} \\
&\quad\quad \times \sqrt{[l,l']}\begin{pmatrix} l & 2 & l' \\ 0 & 0 & 0 \end{pmatrix}\sqrt{I(I+1)(2I+1)}\sqrt{S(S+1)(2S+1)} \\
&\quad\quad \times \begin{pmatrix} 1 & 1 & 2 \\ \Delta M_S & \Delta M_I & \Delta M_l \end{pmatrix}\begin{pmatrix} I & 1 & I' \\ -M_I & \Delta M_I & M'_I \end{pmatrix} \\
&\quad\quad \times \begin{pmatrix} S & 1 & S' \\ -M_S & \Delta M_S & M'_S \end{pmatrix}\begin{pmatrix} l & 2 & l' \\ -M_l & \Delta M_l & M'_l \end{pmatrix}. \qquad \text{(A4)}
\end{aligned}$$

This interaction mixes basis states with different M_S, M_I, and M_l, but it conserves the sum $M_S + M_I + M_l$. Thus, the total angular momentum, M, is also conserved.

In the next step, we consider the asymptotic Hamiltonian, Eq. (4), and we begin with the part of this operator associated with H_2. The rotational term is diagonal in all quantum numbers,

$$\begin{aligned}
&\langle NM_N|\langle IM_I|\langle SM_S|\langle lM_l|\hat{H}_{\mathrm{rot}}|N'M'_N\rangle|IM'_I\rangle|SM'_S\rangle|l'M'_l\rangle \\
&\quad = \delta_{NN'}\delta_{M_NM'_N}\delta_{M_IM'_I}\delta_{M_SM'_S}\delta_{M_lM'_l} \\
&\quad\quad \times \left[B_e N(N+1) - D_v N^2(N+1)^2\right], \qquad \text{(A5)}
\end{aligned}$$

and the matrix elements of the nuclear spin–rotation interaction are given as

$$\begin{aligned}
&-c_{\mathrm{nsr}}\langle NM_N|\langle IM_I|\langle SM_S|\langle lM_l|\hat{\mathbf{N}}\cdot\hat{\mathbf{I}}|N'M'_N\rangle|IM'_I\rangle|SM'_S\rangle|l'M'_l\rangle \\
&\quad = -\delta_{NN'}\delta_{M_SM'_S}\delta_{ll'}\delta_{M_lM'_l}\Big[\delta_{M_IM'_I}\delta_{M_NM'_N}c_{\mathrm{nsr}}M_NM_I \\
&\quad\quad + \delta_{M_NM'_N\pm1}\delta_{M_IM'_I\mp1}\frac{c_{\mathrm{nsr}}}{2}\left(N(N+1)-M'_N(M'_N\pm1)\right)^{1/2} \\
&\quad\quad \times \left(I(I+1)-M'_I(M'_I\mp1)\right)^{1/2}\Big]. \qquad \text{(A6)}
\end{aligned}$$

The intramolecular spin–spin interaction couples (very weakly) states with different rotational angular momenta,

$$\begin{aligned}
&g_{\mathrm{H}}^2\mu_{\mathrm{N}}^2\alpha^2\langle NM_N|\langle IM_I|\langle SM_S|\langle lM_l|\left(\frac{\hat{\mathbf{I}}_1\cdot\hat{\mathbf{I}}_2}{r^3}-\frac{3(\hat{\mathbf{I}}_1\cdot\mathbf{r})(\hat{\mathbf{I}}_2\cdot\mathbf{r})}{r^5}\right)|N'M'_N\rangle|IM'_I\rangle|SM'_S\rangle|l'M'_l\rangle \\
&\quad = \delta_{M_SM'_S}\delta_{ll'}\delta_{M_lM'_l}(-1)^{I-M_I-M'_N}\sqrt{30}c_{\mathrm{dip}}[I]\sqrt{[N,N']}\begin{pmatrix} N & 2 & N' \\ 0 & 0 & 0 \end{pmatrix}\begin{pmatrix} N & 2 & N' \\ -M_N & \Delta M_N & M'_N \end{pmatrix} \\
&\quad\quad \times \begin{pmatrix} I & 2 & I \\ -M_I & \Delta M_I & M'_I \end{pmatrix}\begin{Bmatrix} I_1 & I_1 & 1 \\ I_2 & I_2 & 1 \\ I & I & 2 \end{Bmatrix}\sqrt{I_1(I_1+1)(2I_1+1)I_2(I_2+1)(2I_2+1)}. \qquad \text{(A7)}
\end{aligned}$$

Here, $\begin{Bmatrix} \cdot & \cdot & \cdot \\ \cdot & \cdot & \cdot \\ \cdot & \cdot & \cdot \end{Bmatrix}$ denotes the Wigner 9-j symbol. Both of the Zeeman terms in the asymptotic Hamiltonian of H_2 are diagonal in all quantum numbers,

$$\begin{aligned}
&\langle NM_N|\langle IM_I|\langle SM_S|\langle lM_l|\hat{H}_{\mathrm{Zeeman}}|N'M'_N\rangle|IM'_I\rangle|SM'_S\rangle|l'M'_l\rangle \\
&\quad = -\delta_{NN'}\delta_{M_NM'_N}\delta_{M_IM'_I}\delta_{M_SM'_S}\delta_{M_lM'_l}\mu_N B_Z(1-\sigma) \\
&\quad\quad \times (g_r M_N + g_{\mathrm{H}}M_I). \qquad \text{(A8)}
\end{aligned}$$

The same applies to the asymptotic Hamiltonian of lithium from Eq. (9),

$$\begin{aligned}
&\langle NM_N|\langle IM_I|\langle SM_S|\langle lM_l|\hat{H}_{\mathrm{Li}}|N'M'_N\rangle|IM'_I\rangle|SM'_S\rangle|l'M'_l\rangle \\
&\quad = -\delta_{NN'}\delta_{M_NM'_N}\delta_{M_IM'_I}\delta_{M_SM'_S}\delta_{M_lM'_l}g_S\mu_B B_Z M_S. \qquad \text{(A9)}
\end{aligned}$$

APPENDIX B: MATRIX ELEMENTS IN EQ. (11)—THE BASIS WITH COUPLED H_2 VECTORS

Similarly to the uncoupled case, the H_2–Li interaction is diagonal in M_S,

$$\begin{aligned}
&\langle (NI)FM_F|\langle SM_S|\langle lM_l|\hat{V}(\mathbf{R},\mathbf{r})|(N'I)F'M'_F\rangle|SM'_S\rangle|l'M'_l\rangle \\
&\quad = \delta_{M_SM'_S}(-1)^{M'_l-M_F+I+F+F'}\sqrt{[N,N',l,l',F,F']} \\
&\quad\quad \times \sum_{\lambda=0}^{\lambda_{\max}} v^{N,N'}_{\lambda,v=0}(R)\begin{pmatrix} l & \lambda & l' \\ 0 & 0 & 0 \end{pmatrix}\begin{pmatrix} l & \lambda & l' \\ -M_l & \Delta M_l & M'_l \end{pmatrix}\begin{pmatrix} N & \lambda & N' \\ 0 & 0 & 0 \end{pmatrix} \\
&\quad\quad \times \begin{pmatrix} F & \lambda & F' \\ -M_F & \Delta M_F & M'_F \end{pmatrix}\begin{Bmatrix} N' & F' & I \\ F & N & \lambda \end{Bmatrix}. \qquad \text{(B1)}
\end{aligned}$$

The spin-dependent interaction is diagonal in N,

$$\begin{aligned}
&\langle (NI)FM_F|\langle SM_S|\langle lM_l|\hat{V}_{\mathrm{SD}}(\mathbf{R},\mathbf{r},\hat{\mathbf{I}},\hat{\mathbf{S}})|(N'I)F'M_F'\rangle|SM_S'\rangle|l'M_l'\rangle \\
&= \delta_{NN'} g_S \mu_B g_{\mathrm{H}} \mu_N \left(\frac{\alpha^2}{R^3}\right) \sqrt{30}(-1)^{M_l+I+N+F} \sqrt{[l,l',F,F']} \\
&\times \begin{pmatrix} l & 2 & l' \\ 0 & 0 & 0 \end{pmatrix} \sqrt{I(I+1)(2I+1)} \sqrt{S(S+1)(2S+1)} \\
&\times \begin{pmatrix} 1 & 1 & 2 \\ \Delta M_F & \Delta M_S & \Delta M_l \end{pmatrix} \begin{pmatrix} F & 1 & F' \\ -M_F & \Delta M_F & M_F' \end{pmatrix} \\
&\times \begin{pmatrix} S & 1 & S' \\ -M_S & \Delta M_S & M_S' \end{pmatrix} \begin{pmatrix} l & 2 & l' \\ -M_l & \Delta M_l & M_l' \end{pmatrix} \begin{Bmatrix} I & F' & N \\ F & I & 1 \end{Bmatrix}.
\end{aligned} \tag{B2}$$

The rotational part of the Hamiltonian is diagonal in all quantum numbers,

$$\begin{aligned}
&\langle (NI)FM_F|\langle SM_S|\langle lM_l|\hat{H}_{\mathrm{rot}}|(N'I)F'M_F'\rangle|SM_S'\rangle|l'M_l'\rangle \\
&= \delta_{NN'}\delta_{FF'}\delta_{M_FM_F'}\delta_{M_SM_S'}\delta_{M_lM_l'} \\
&\times \left(B_e N(N+1) - D_v N^2 (N+1)^2\right).
\end{aligned} \tag{B3}$$

Both hyperfine interactions are diagonal in the total angular momentum of H_2 and its projection on the space-fixed Z-axis. The nuclear spin–rotation interaction is additionally diagonal in all other quantum numbers,

$$\begin{aligned}
&-c_{\mathrm{nsr}}\langle (NI)FM_F|\langle SM_S|\langle lM_l|\hat{\mathbf{N}}\cdot\hat{\mathbf{I}}|(N'I)F'M_F'\rangle|SM_S'\rangle|l'M_l'\rangle \\
&= -\delta_{NN'}\delta_{FF'}\delta_{M_FM_F'}\delta_{M_SM_S'}\delta_{M_lM_l'}\frac{c_{\mathrm{nsr}}}{2} \\
&\times (F(F+1) - I(I+1) - N(N+1)).
\end{aligned} \tag{B4}$$

The spin–spin magnetic dipole interaction can, in principle, couple states with different N and I. This coupling is 11 orders of magnitude smaller than the spacing between the N and $N' = N \pm 2$ rotational states of H_2, and we neglect it here. We additionally neglect any *ortho*-/*para*-H_2 coupling. The matrix elements of this interaction are

$$\begin{aligned}
&g_{\mathrm{H}}^2\mu_{\mathrm{N}}^2\alpha^2\langle (NI)FM_F|\langle SM_S|\langle lM_l|\left(\frac{\hat{\mathbf{I}}_1\cdot\hat{\mathbf{I}}_2}{r^3} - \frac{3(\hat{\mathbf{I}}_1\cdot\mathbf{r})(\hat{\mathbf{I}}_2\cdot\mathbf{r})}{r^5}\right)|(N'I)F'M_F'\rangle|SM_S'\rangle|l'M_l'\rangle \\
&= -\delta_{M_SM_S'}\delta_{ll'}\delta_{FF'}\delta_{M_FM_F'}(-1)^{N+N'+I+F}\sqrt{30}c_{\mathrm{dip}}[I]\sqrt{[N,N']} \\
&\times \begin{pmatrix} N & 2 & N' \\ 0 & 0 & 0 \end{pmatrix} \begin{Bmatrix} N & N' & 2 \\ I & I & F \end{Bmatrix} \begin{Bmatrix} I_1 & I_1 & 1 \\ I_2 & I_2 & 1 \\ I & I & 2 \end{Bmatrix} \sqrt{I_1(I_1+1)(2I_1+1)I_2(I_2+1)(2I_2+1)}.
\end{aligned} \tag{B5}$$

The matrix elements of the Zeeman term of the lithium atom are identical to those given by Eq. (A8). Finally, the Zeeman Hamiltonian of H_2 has the following matrix elements:

$$\begin{aligned}
&\langle (NI)FM_F|\langle SM_S|\langle lM_l|\hat{H}_{\mathrm{Zeeman}}|(N'I)F'M_F'\rangle|SM_S'\rangle|l'M_l'\rangle \\
&= \delta_{NN'}\delta_{M_SM_S'}\delta_{M_lM_l'}\mu_N B_Z(1-\sigma)(-1)^{F'-m_F+I+N'+F'} \\
&\times \begin{pmatrix} F & 1 & F' \\ -M_F & 0 & M_F' \end{pmatrix} \sqrt{[F,F']} \sqrt{I(I+1)(2I+1)} \\
&\times \left(\delta_{NN'} g_r \begin{Bmatrix} F & F' & 1 \\ I & I & N \end{Bmatrix} + g_{\mathrm{H}} \begin{Bmatrix} F & F' & 1 \\ N' & N & I \end{Bmatrix}\right).
\end{aligned} \tag{B6}$$

REFERENCES

[1] R. V. Krems, Phys. Chem. Chem. Phys. **10**, 4079 (2008).
[2] N. Balakrishnan, J. Chem. Phys. **145**, 150901 (2016).
[3] M. Tizniti, S. D. Le Picard, F. Lique, C. Berteloite, A. Canosa, M. H. Alexander, and I. R. Sims, Nat. Chem. **6**, 141 (2014).
[4] A. B. Henson, S. Gersten, Y. Shagam, J. Narevicius, and E. Narevicius, Science **338**, 234 (2012).
[5] E. Lavert-Ofir, Y. Shagam, A. B. Henson, S. Gersten, J. Kłos, P. S. Żuchowski, J. Narevicius, and E. Narevicius, Nat. Chem. **6**, 332 (2014).
[6] Y. Shagam, A. Klein, W. Skomorowski, R. Yun, V. Averbukh, C. P. Koch, and E. Narevicius, Nat. Chem. **7**, 921 (2015).
[7] A. Klein, Y. Shagam, W. Skomorowski, P. S. Żuchowski, M. Pawlak, L. M. C. Janssen, N. Moiseyev, S. Y. T. van de Meerakker, A. van der Avoird, C. P. Koch, and E. Narevicius, Nat. Phys. **13**, 35 (2016).
[8] W. E. Perreault, N. Mukherjee, and R. N. Zare, Science **358**, 356 (2017).
[9] W. E. Perreault, N. Mukherjee, and R. N. Zare, Nat. Chem. **10**, 561 (2018).
[10] H. Zhou, W. E. Perreault, N. Mukherjee, and R. N. Zare, Science **374**, 960 (2021).
[11] H. Zhou, W. E. Perreault, N. Mukherjee, and R. N. Zare, J. Chem. Phys. **154**, 104309 (2021).
[12] P. G. Jambrina, J. F. E. Croft, H. Guo, M. Brouard, N. Balakrishnan, and F. J. Aoiz, Phys. Rev. Lett. **123**, 043401 (2019).
[13] A. Devolder, T. Tscherbul, and P. Brumer, Phys. Rev. A **102**, 031303 (2020).
[14] A. Devolder, P. Brumer, and T. V. Tscherbul, Phys. Rev. Lett. **126**, 153403 (2021).
[15] N. Balakrishnan, R. Forrey, and A. Dalgarno, Chem. Phys. Lett. **280**, 1 (1997).
[16] N. Balakrishnan, R. C. Forrey, and A. Dalgarno, Phys. Rev. Lett. **80**, 3224 (1998).
[17] A. Mack, T. K. Clark, R. C. Forrey, N. Balakrishnan, T.-G. Lee, and P. C. Stancil, Phys. Rev. A **74**, 052718 (2006).
[18] G. Quéméner, N. Balakrishnan, and R. V. Krems, Phys. Rev. A **77**, 030704 (2008).
[19] G. Quéméner and N. Balakrishnan, J. Chem. Phys. **130**, 114303 (2009).
[20] N. Balakrishnan, G. Quéméner, R. C. Forrey, R. J. Hinde, and P. C. Stancil, J. Chem. Phys. **134**, 014301 (2011).

[21] S. F. dos Santos, N. Balakrishnan, S. Lepp, G. Quéméner, R. C. Forrey, R. J. Hinde, and P. C. Stancil, J. Chem. Phys. **134**, 214303 (2011).
[22] J. F. E. Croft, N. Balakrishnan, M. Huang, and H. Guo, Phys. Rev. Lett. **121**, 113401 (2018).
[23] J. F. E. Croft and N. Balakrishnan, J. Chem. Phys. **150**, 164302 (2019).
[24] M. Morita and N. Balakrishnan, J. Chem. Phys. **153**, 091101 (2020).
[25] P. G. Jambrina, M. Morita, J. F. E. Croft, F. J. Aoiz, and N. Balakrishnan, J. Phys. Chem. Lett. **13**, 4064 (2022).
[26] N. F. Ramsey, Phys. Rev. **85**, 60 (1952).
[27] H. Jóźwiak, H. Cybulski, and P. Wcisło, J. Quant. Spectrosc. Radiat. Transfer **253**, 107186 (2020).
[28] M. Puchalski, J. Komasa, and K. Pachucki, Phys. Rev. Lett. **125**, 253001 (2020).
[29] A. Fast and S. A. Meek, Phys. Rev. Lett. **125**, 023001 (2020).
[30] A. Fast and S. A. Meek, Mol. Phys. **120**, e1999520 (2021).
[31] J. Komasa, M. Puchalski, P. Czachorowski, G. Łach, and K. Pachucki, Phys. Rev. A **100**, 032519 (2019).
[32] M. Puchalski, J. Komasa, P. Czachorowski, and K. Pachucki, Phys. Rev. Lett. **122**, 103003 (2019).
[33] M. Zaborowski, M. Słowiński, K. Stankiewicz, F. Thibault, A. Cygan, H. Jóźwiak, G. Kowzan, P. Masłowski, A. Nishiyama, N. Stolarczyk, S. Wójtewicz, R. Ciuryło, D. Lisak, and P. Wcisło, Opt. Lett. **45**, 1603 (2020).
[34] W. Ubachs, J. Koelemeij, K. Eikema, and E. Salumbides, J. Mol. Spectrosc. **320**, 1 (2016).
[35] M. L. Diouf, F. M. J. Cozijn, B. Darquié, E. J. Salumbides, and W. Ubachs, Opt. Lett. **44**, 4733 (2019).
[36] T.-P. Hua, Y. R. Sun, and S.-M. Hu, Opt. Lett. **45**, 4863 (2020).
[37] S. Kassi, C. Lauzin, J. Chaillot, and A. Campargue, Phys. Chem. Chem. Phys. **24**, 23164 (2022).
[38] F. M. J. Cozijn, M. L. Diouf, and W. Ubachs, Eur. Phys. J. D **76**, 220 (2022).
[39] Q.-H. Liu, Y.-N. Lv, C.-L. Zou, C.-F. Cheng, and S.-M. Hu, Phys. Rev. A **106**, 062805 (2022).
[40] H. Jóźwiak and P. Wcisło, Sci. Rep. **12**, 14529 (2022).
[41] A. Singh, L. Maisenbacher, Z. Lin, J. J. Axelrod, C. D. Panda, and H. Müller, Phys. Rev. Res. **5**, 033008 (2023).
[42] M. Lara, J. L. Bohn, D. Potter, P. Soldán, and J. M. Hutson, Phys. Rev. Lett. **97**, 183201 (2006).
[43] M. Lara, J. L. Bohn, D. E. Potter, P. Soldán, and J. M. Hutson, Phys. Rev. A **75**, 012704 (2007).
[44] T. V. Tscherbul, J. Kłos, and A. A. Buchachenko, Phys. Rev. A **84**, 040701(R) (2011).
[45] M. Morita, J. Kłos, A. A. Buchachenko, and T. V. Tscherbul, Phys. Rev. A **95**, 063421 (2017).
[46] L. D. Carr, D. DeMille, R. V. Krems, and J. Ye, New J. Phys. **11**, 055049 (2009).
[47] P. M. Duarte, R. A. Hart, J. M. Hitchcock, T. A. Corcovilos, T.-L. Yang, A. Reed, and R. G. Hulet, Phys. Rev. A **84**, 061406 (2011).
[48] C. Makrides, D. S. Barker, J. A. Fedchak, J. Scherschligt, S. Eckel, and E. Tiesinga, Phys. Rev. A **99**, 042704 (2019).
[49] R. V. Krems and A. Dalgarno, J. Chem. Phys. **120**, 2296 (2004).
[50] A. Volpi and J. L. Bohn, Phys. Rev. A **65**, 052712 (2002).
[51] R. Hermsmeier, X. Xing, and T. V. Tscherbul, J. Phys. Chem. A **127**, 4511–4525 (2023).
[52] J. M. Brown and A. Carrington, *Rotational Spectroscopy of Diatomic Molecules* (Cambridge University Press, 2003).
[53] T. V. Tscherbul, P. Zhang, H. R. Sadeghpour, and A. Dalgarno, Phys. Rev. A **79**, 062707 (2009).
[54] T. V. Tscherbul, P. Zhang, H. R. Sadeghpour, and A. Dalgarno, Phys. Rev. Lett. **107**, 023204 (2011).
[55] I. C. Bowater, J. M. Brown, and A. Carrington, Proc. R. Soc. London, Ser. A **333**, 265 (1973).
[56] J. M. Cook, G. W. Hills, and R. F. Curl, J. Chem. Phys. **67**, 1450 (1977).
[57] L. H. Coudert, W. E. Ernst, and O. Golonzka, J. Chem. Phys. **117**, 7102 (2002).
[58] A. W. Hauser, J. V. Pototschnig, and W. E. Ernst, Chem. Phys. **460**, 2 (2015).
[59] S. Upadhyay, U. Dargyte, V. D. Dergachev, R. P. Prater, S. A. Varganov, T. V. Tscherbul, D. Patterson, and J. D. Weinstein, Phys. Rev. A **100**, 063419 (2019).
[60] A. van der Avoird and G. Brocks, J. Chem. Phys. **87**, 5346 (1987).
[61] L. M. C. Janssen, P. S. Żuchowski, A. van der Avoird, J. M. Hutson, and G. C. Groenenboom, J. Chem. Phys. **134**, 124309 (2011).
[62] Y. V. Suleimanov, T. V. Tscherbul, and R. V. Krems, J. Chem. Phys. **137**, 024103 (2012).
[63] T. V. Tscherbul, J. Kłos, L. Rajchel, and R. V. Krems, Phys. Rev. A **75**, 033416 (2007).
[64] B. Johnson, J. Comput. Phys. **13**, 445–449 (1973).
[65] R. N. Zare and W. G. Harter, *Angular Momentum: Understanding Spatial Aspects in Chemistry and Physics* (Wiley-Interscience Publication, New York, 1988).
[66] K. P. Huber and G. Herzberg, *Molecular Spectra and Molecular Structure* (Springer, 1979).
[67] K. Pachucki and J. Komasa, Phys. Rev. A **83**, 032501 (2011).
[68] 2018 CODATA recommended values" (2018).
[69] D. Sundholm, J. Gauss, and A. Schäfer, J. Chem. Phys. **105**, 11051 (1996).
[70] J. L. Booth, P. Shen, R. V. Krems, and K. W. Madison, New J. Phys. **21**, 102001 (2019).
[71] P. Shen, E. Frieling, K. R. Herperger, D. Uhland, R. A. Stewart, A. Deshmukh, R. V. Krems, J. L. Booth, and K. W. Madison, New J. Phys. **25**, 053018 (2023).
[72] J. Kłos and E. Tiesinga, J. Chem. Phys. **158**, 014308 (2023).
[73] D. E. Manolopoulos, J. Chem. Phys. **85**, 6425–6429 (1986).
[74] E. P. Wigner, Phys. Rev. **73**, 1002 (1948).
[75] S. Koyu, R. Hermsmeier, and T. V. Tscherbul, J. Chem. Phys. **156**, 034112 (2022).
[76] P. Jacobs, *Group Theory with Applications in Chemical Physics* (Cambridge University Press, 2005).
[77] D. W. Schwenke, J. Chem. Phys. **89**, 2076 (1988).